Macromolecules

ARTICLE

pubs.acs.org/Macromolecules

Theory of Tethered Polymers in Shear Flow: The Strong Stretching Limit

Charles E. Sing and Alfredo Alexander-Katz*

Department of Materials Science and Engineering, Massachusetts Institute of Technology, Cambridge, Massachusetts 02139, United States

ABSTRACT: In the present article, we use simulation and theory to understand the case of flexible and semiflexible tethered polymers in the limit of high shear flows and consequently near-full extension of the chains. We adopt a random-walk picture along the axis of the polymer, which in combination with a statistical mechanical description of perturbations along the chain contour allows us to fully characterize the geometry of the polymer chain without any fit parameters. Incorporation of hydrodynamic interactions is also investigated, with the hydrodynamic lift force inducing changes in the chain equilibrium structure near the tether point that could have implications for adsorption and desorption kinetics.

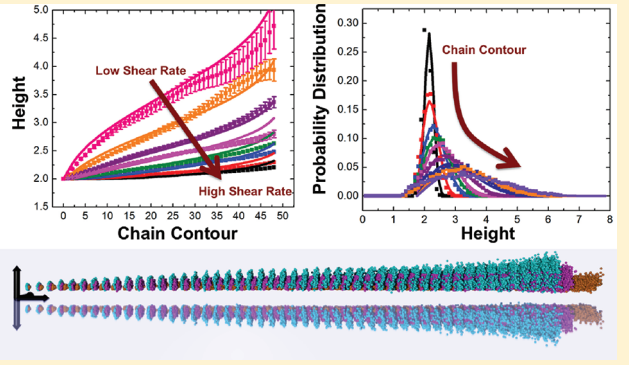

INTRODUCTION

Polymer chains that are tethered to a surface by one end and extend outward into a fluid medium serve as a model system that has many well-known implications, particularly in the fields of polymer surface functionalization and microfulidics.[1−10] It is part of the broader field interested in characterizing the interactions between polymers and surfaces, a motif which is ubiquitous in polymer physics.[11−17] Early work on tethered polymer chains was performed by De Gennes in the context of a larger paper on polymer brushes, who described their geometry using typical Gaussian polymer statistics.[15] The addition of a fluid flow was further investigated by Brochard-Wyart, who used a scaling Pincus-blob picture to describe the extended polymer chain.[18] Extension of this picture to the case of a collapsed polymer globule is considered by the same author, who described the existence of a "trumpet" structure.[12]

Experimental investigation of tethered polymers in shear was made possible by the introduction of fluorescently labeled DNA molecules, and drove a resurgence of interest in this phenomenon.[19,20] These polymers can be placed in flows controlled by microfluidic channels, and studied via fluorescence microscopy. Initial work was largely performed by Doyle et al. who tackled the problem with a combination of experiment, simulation, and theory.[3,21] It was found that the extension of the polymer, given by the reduced extension parameter $\varepsilon = 1 - R/L$ (where L is the chain contour length and R is the projection of the chain along the flow direction) is linked by a simple scaling law to the Weissenberg number Wi, which is a dimensionless number that compares the rate of shear flow $\dot{\gamma}$ to the characteristic relaxation time of the polymer τ_R.[3,21] Using a free-draining approximation, the result for a worm-like chain (WLC) is $\varepsilon \sim Wi^{-1/3}$ and for a freely jointed chain (FJC) is $\varepsilon \sim Wi^{-2/3}$.[3,21] The WLC results appear to match the trends seen in experiments.[3,21]

Subsequent work on the behavior of tethered polymers has focused on the dynamic aspects first observed in the work of Doyle et al. where the end of a tethered chain appears to undergo cyclic motion[3,22−26] that is reminiscent of the "tumbling" behavior seen in free polymers in shear flow.[20,27−29] This is explained as a coupling between thermal fluctuations and the spatial variation in the fluid flows, and the spectral behavior of this process has been widely studied.[3,20,22−26] This effect has been recently called into question, however, due to the reproduction of the same trends using simple dimer models.[24]

Beyond the initial work by Doyle et al., there has been little further discussion of the equilibrium structure of a tethered chain in fluid flow. One notable exception was a study by Serr and Netz on the structure of polymers undergoing deformation due to pulling forces at one end of the chain, and the consequences this has on adsorption propensity.[14] This situation is equivalent to tethered polymers in uniform flow; however, surface confinement and hydrodynamic interactions were neglected in the aforementioned study.[14] In general there has been little investigation into the role of hydrodynamic interactions, particularly hydrodynamic lift forces, on the equilibrium structure of the chain. This is widely dismissed as being of little importance on the overall equilibrium structure, due to the elongated nature of the polymer chain, and therefore only the effect on relaxation time (Rouse versus Zimm relaxation) is considered.[22] In this article, we develop a theory to supplement the initial work by Doyle et al. by considering a chain in the near-full extension limit. In this case, we utilize a novel approach that treats the trajectory of the chain as a random walk of perturbations from a completely stretched ground state whose step size is a strong function of

Received: August 6, 2011
Revised: October 5, 2011
Published: October 25, 2011

both the strength of the shear flow and the contour coordinate of a given monomer. We utilize both theory and simulation to develop this analytical description, and demonstrate how different conditions, in particular semiflexibility, may be incorporated into this overall picture. We finally consider the effect of hydrodynamic interactions, and utilize recent theories on the hydrodynamic lift force to show that there is indeed a drastic change in chain equilibrium structure at the tether point.[11] All theoretical results presented in this paper require no fit parameters, and thus provide a quantitative description of the chain equilibrium structure.

Understanding tethered polymers in this limit has important implications in understanding the dynamics of a flow-induced adsorption/desorption transition, since this can often occur at this high-flow limit.[14,16,30] Previous work has demonstrated a nuanced competition between hydrodynamic lift forces and a flow-induced "flattening" effect, and thus it is reasonable to assume that this case represents a likely transition state between an adsorbed and desorbed chain.[14,16,31] In particular, we postulate the presence of a hydrodynamic lift force at the tether point which may drive the desorption process through an "unzipping" mechanism.

Furthermore, it is beneficial to have a detailed understanding of tethered chain geometries for a wide range of applications. For example, tethered polymers are often used as decoration to impart chemical functionality or physical properties on biopolymer surfaces.[6−8] This functionality is often coupled directly to chain conformations,[6−8] which we demonstrate in this article can be predicted in the presence of simple shear. The ability to know the spatial distribution of, for example, the chain end as a function of shear could lead to predictive models of how ligand-decorated surfaces interact with their surroundings in flows.[8] The case of a tethered molecule is also important in the context of single-molecule manipulation, which specifically aims to use flow to dictate molecular conformations in a controllable way for technologies such as DNA sorting or molecular-level device creation.[9,10] In these applications, it is vital that a complete and accurate description of the conformational behaviors and hydrodynamic forces is available.

SIMULATION METHODS

We use a Brownian dynamics bead−spring model to represent a polymer chain tethered at a surface. To do this, we consider N beads that reside in a potential U that is a function of the springs connecting each bead, the excluded volume of neighboring beads, an optional bending energy term, and the excluded volume of the wall. The form of this is given as:

$$\tilde{U} = \frac{\tilde{\kappa}}{2}\sum_{i=1}^{N-1}(\tilde{r}_{i+1,i}-2)^2 + \tilde{u}\sum_{ij}\left(\left(\frac{2}{\tilde{r}_{i,j}}\right)^{12} - 2\left(\frac{2}{\tilde{r}_{i,j}}\right)^{6}\right) + \frac{\tilde{\kappa}_B}{2}\sum_{i=1}^{N-1}(\theta_{i+1}-\theta_i)^2 + \tilde{U}_{wall} \quad (1)$$

where $\tilde{U} = U/kT$ is a dimensionless energy, $\tilde{\kappa} = \kappa a^2/kT$ is a dimensionless spring constant, $\tilde{\kappa}_B = \kappa_B a^2/kT$ is the bending spring constant between two adjacent links at angles θ_{i+1} and θ_i, $\tilde{r}_{i,j} = r/a$ is the dimensionless distance between bead I and j, and $\tilde{U}_{wall}$ is the wall potential given by:

$$\tilde{U}_{wall} = \begin{cases} -4\ln(\tilde{z}-1) + 4\tilde{z} - 8 & \tilde{z} < 2 \\ 0 & \tilde{z} \geq 2 \end{cases} \quad (2)$$

We note that this potential diverges at $\tilde{z} = 1$ since the center of mass of a bead of radius $\tilde{a} = 1$ that is flush with the surface at $\tilde{z} = 0$ is at $\tilde{z} = 1$. This is a soft potential that only takes effect at points very close to the surface. It has been verified that the exact shape of this potential has no profound effect on the properties of the tethered chain, so long as the potential remains repulsive and local. The tether point was created by fixing the position of the first bead of the chain at $\tilde{x} = \tilde{y} = 0$ and $\tilde{z} = 2$. In general, all values designated with a tilde are dimensionless, with all distances normalized by a, all energies normalized by kT, and all times normalized by the characteristic diffusion time of an individual monomer $\tau_0 = 6\pi\eta a^3/(kT)$.

This potential is used as an input to the Langevin equation, which describes the motion of a bead i at position $\tilde{\mathbf{r}}_i$:

$$\frac{\partial\tilde{\mathbf{r}}_i}{\partial\tilde{t}} = \tilde{\mathbf{v}}_\infty(\tilde{\mathbf{r}}_i) - \sum_j(\tilde{\mu}_{ij}\nabla_{\mathbf{r}_j}\tilde{U}(\tilde{t}) + \nabla_{\tilde{\mathbf{r}}_i}\cdot\tilde{\mathbf{D}}_{ij}) + \tilde{\xi}_i(\tilde{t}) \quad (3)$$

where $\tilde{\mathbf{v}}_\infty(\tilde{\mathbf{r}}_i) = \tilde{\dot{\gamma}}\tilde{r}_{i,z}\hat{\mathbf{x}}$ is the solvent flow profile (in this case, simple shear, where $\tilde{\dot{\gamma}}$ is the shear rate magnitude and $\hat{\mathbf{x}}$ is a unit vector in the x-direction). $\tilde{\xi}_i$ is a random velocity that satisfies $\langle\tilde{\xi}_i(\tilde{t})\tilde{\xi}_j(\tilde{t}')\rangle = 2\tilde{\mu}\delta(\tilde{t}-\tilde{t}')$, and $\mathbf{D} = k_BT\mu_{ij}$ such that $\tilde{\mathbf{D}} = \tilde{\mu}_{ij}\cdot\tilde{\mu}_{ij}$ is the mobility matrix, which in our simulations is represented in one of two different ways: with and without hydrodynamic interactions (HI). The non-HI case is known as the Freely−Draining approximation (FD), which dictates that each bead of radius a feels a constant drag coefficient given by the Stokes mobility $\mu_0 = 1/(6\pi\eta_S a)$, where η_S is the solvent viscosity. In the dimensionless case, the mobility thus becomes simply $\tilde{\mu}_{ij} = \mathbf{I}\delta_{ij}$. In the HI case, we represent the mobility matrix in the form known as the Blake−Rotne−Prager tensor, which is given in a large number of references.[1,5,16,32−35] Conceptually, the Blake−Rotne−Prager tensor considers hydrodynamic interactions between finite-size beads in a low-Reynolds number solvent in the vicinity of a surface, and has been shown to correlate extremely well with experiment.[1,5,16,32−36] By considering both the FD and HI conditions, we gain insight into the influence of HI on the equilibrium structure of a tethered polymer.

We organize this paper into two main sections: first we present a theory section where we derive the main theoretical results, and there is a subsequent discussion section comparing the theory to simulation results. We finalize the paper with our conclusions and future prospects.

THEORY OF STRONGLY-STRETCHED CHAINS

To develop this theory, we first derive the most simple case of a freely jointed chain (FJC) with no hydrodynamic interactions (HI). The incorporation of semiflexibility (WLC characteristics) and HI will be subsequently considered.

FJC, No HI. The overall picture of a tethered chain in the highly stretched limit is demonstrated in Figure 1. We assume a geometry of a stretched chain that is in a ground state that is completely straight chain of N beads of radius a that is tethered at a distance z_0 from the surface. The surface is at a height $z = 0$ and extends outward in the $x - y$ plane. Viewing the polymer chain along its fully stretched axis, we can consider perturbations of a

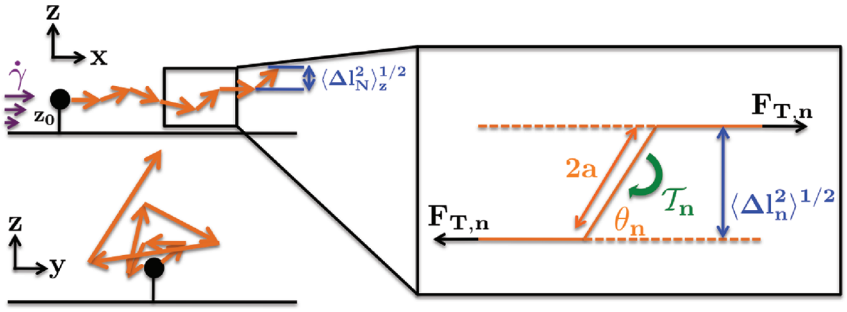

Figure 1. Schematic demonstrating the geometry of the tethered chain and the definition of the relevant variables. When a tethered chain beginning at height z_0 from the surface consisting of N links separated by distance $2a$ is in a strong simple shear flow, the chain lies roughly parallel to the surface plane in a direction here defined as the x direction (top left). In the $z - y$ plane, the chain appears to undergo a random walk from the tether point with increasing step size $\langle \Delta l_n^2 \rangle$ with increasing n (bottom left). In this theory, this distance $\langle \Delta l_n^2 \rangle$ is calculated by developing an analytical expression for the partition function of an individual link as it undergoes an angular perturbation θ_n from the horizontal ground state (right). This energy associated with this is due to the torque $\mathcal{J}_n$ applied by the chain tensile force $F_{T,n}$. A bending energy constant κ_B can also be introduced to consider correlations between adjacent values of θ_n.

given link of index n, where n goes from 1 to N along the z and y directions with a distance of magnitude Δl_z and Δl_y respectively. Locally, these perturbations are essentially cylindrically symmetric, and constitute a randomly oriented step of length $\Delta l(n)$, which is a function of the distance along the polymer contour n. From this perspective, the geometry of the polymer can be described as a random walk from the tether point at height z_0, and its time-averaged equilibrium distribution function in the z-direction can be described by the straightforward solution of the diffusion equation that describes a point source near a surface. The form of this equation is the traditional Gaussian distribution centered around z_0 with an image distribution at $-z_0$ to account for the no-flux and complete depletion boundary conditions at a surface at $z = 0$:

$$P(z,n,\dot{\gamma},z_0,\{z_n\}) = C(e^{-(z-z_0)^2/2S_n[\dot{\gamma},\{z_n\}]} - e^{-(z+z_0)^2/2S_n[\dot{\gamma},\{z_n\}]}) \quad (4)$$

where $P(z,n,\dot{\gamma},z_0,\{z_n\})$ is the probability distribution function in the z-direction, C is a normalization constant, $\dot{\gamma}$ is the shear rate, and $S_n[\dot{\gamma},\{z_n\}]$ is a functional that describes the width of the distribution along a given direction (for a simple Gaussian distribution, this would be the square of the variance):

$$S_n[\dot{\gamma},\{z_n\}] = \frac{1}{2}\int_0^n \langle \Delta l^2 \rangle (n',\dot{\gamma},z_{n'})\, dn' \quad (5)$$

where $\langle \Delta l^2 \rangle (n',\dot{\gamma},z_{n'})$ is the mean squared displacement at index n' and $\{z_n\}$ is the set of z coordinates for every bead index n. We note that, if $\langle \Delta l^2 \rangle$ is constant, we retain the well-known result for a random walk $S_n[\dot{\gamma},\{z_n\}] = n\langle \Delta l^2 \rangle$. For the case of a tethered chain, however, $\langle \Delta l^2 \rangle$ is a function of the location along the contour of the chain as demonstrated in Figure 1.

In the case of a FJC, we expect the major driving force toward the completely stretched ground state is the tensile force F_T along the chain (as opposed to chain rigidity, which we will account for in the next section). Figure 1 provides a schematic of this driving force, which can be described as a torque $\mathcal{J}_T$ that is a function of the bond angle with relation to the surface plane θ. This is given by:

$$\mathcal{J}_{T,n} = -2F_{T,n}\sin\theta_n a \quad (6)$$

where we have introduced the subscript n to reinforce that these are local variables that can change as a value of position along the chain contour n. This can be integrated over θ_n to yield the associated energy U_n:

$$\tilde{U}_n = \int_0^{\theta_n} 2\tilde{F}_{T,n} \sin\theta_n' d\theta_n' \approx \tilde{F}_{T,n}\theta_n^2 \quad (7)$$

where we have now replaced all values by their dimensionless counterparts. The end result of the above equation is due to the crucial approximation in this treatment of the tethered polymer, which is that θ_n always remains small. This will be true only in the high shear limit, and this is ultimately what prevents this approach from being relevant over all values of $\dot{\gamma}$. This approximation is necessary to develop an analytical partition function q_n of bond n, which is given by

$$q_n = \int_0^{\pi/2} e^{\ln\theta_n - \tilde{U}_n}\, d\theta_n \approx \int_0^{\infty} \theta_n e^{-\tilde{F}_{T,n}\theta_n^2}\, d\theta_n = \frac{1}{2\tilde{F}_{T,n}} \quad (8)$$

where we have assumed that $\tilde{F}_{T,n}$ is large enough that the upper limit in the integral can be taken as ∞ rather than $\pi/2$. We include an entropic term $\ln\theta_n$ that accounts for the linear increase of degeneracy with θ_n. It is straightforward to calculate $\langle \Delta\tilde{l}^2 \rangle_n$ with this approach:

$$\langle \Delta\tilde{l}^2 \rangle_n \approx \frac{4}{q_n}\int_0^{\infty} \theta^3 e^{-\tilde{F}_{T,n}\theta_n^2}\, d\theta_n = \frac{4}{\tilde{F}_{T,n}} \quad (9)$$

The only variable thus required is the tensile force $\tilde{F}_{T,n}$ at index n. In its most general form $\tilde{F}_{T,n}$ is a functional $\tilde{F}_{T,n}[\dot{\gamma},\{z_n\}]$ that depends on the overall contour of the chain:

$$\tilde{F}_{T,n}[\dot{\gamma},\{z_n\}] = \int_n^N \tilde{F}_{F,n'}(\dot{\gamma},z_{n'})\, dn' \quad (10)$$

where $\tilde{F}_{F,n}(\dot{\gamma},z_{n'})$ is the force exerted by the flow on a bead of index n'. Thus, the tension force at a given point along the chain is determined by the trajectory of the chain beyond that point. This is difficult to solve in an analytic fashion, however in the limit of highly stretched chains we can assume that the trajectory will be nearly flat along the surface. This means that there is some average height $\bar{d}$ that remains roughly constant along the length of the entire chain. By assuming this geometry, we obtain a simple relationship for the fluid force on a given location along

the chain:

$$\tilde{F}_{F,n'} = \tilde{\mu}^{-1}\tilde{\dot{\gamma}}\,\tilde{d} = \tilde{\dot{\gamma}}\,\tilde{d} \tag{11}$$

where we are dealing with the FD case, $\tilde{\mu} = 1$. We can then create a final form for $\langle \Delta\tilde{l}^2 \rangle_{n,z}$:

$$\langle \Delta\tilde{l}^2 \rangle_{n,z} = \frac{4}{\tilde{\dot{\gamma}}\,\tilde{d}(N-n)} \tag{12}$$

This is incorporated into the equation for $S_n[\dot{\gamma},\{\tilde{z}_n\}]$:

$$S_n[\dot{\gamma},\{\tilde{z}_n\}] = \frac{1}{2}\int_0^n \frac{4}{\tilde{\dot{\gamma}}\,\tilde{d}(N-n')}\,\mathrm{d}n' = \frac{2}{\tilde{\dot{\gamma}}\,\tilde{d}}\ln\left[\frac{N}{N-n}\right] \tag{13}$$

and finally:

$$P(\tilde{z},n,\dot{\gamma},\tilde{z}_0) = C(\mathrm{e}^{-(\tilde{z}-\tilde{z}_0)^2/\{4/\tilde{\dot{\gamma}}\,\tilde{d}\}\{\ln[N/(N-n)]\}} - \mathrm{e}^{-(\tilde{z}+\tilde{z}_0)^2/\{4/\tilde{\dot{\gamma}}\,\tilde{d}\}\{\ln[N/(N-n)]\}}) \tag{14}$$

A final form of this probability enables the calculation of the mean trajectory of the polymer:

$$\langle \tilde{z} \rangle(n) = \frac{\int_0^\infty \tilde{z}P(\tilde{z},n,\tilde{\dot{\gamma}},\tilde{z}_0)\,\mathrm{d}\tilde{z}}{\int_0^\infty P(\tilde{z},n,\tilde{\dot{\gamma}},\tilde{z}_0)\,\mathrm{d}\tilde{z}} = \tilde{z}_0\left(\mathrm{erf}\left[\frac{\tilde{z}_0}{\sqrt{\frac{4}{\tilde{\dot{\gamma}}\,\tilde{d}}\ln\left[\frac{N}{N-n}\right]}}\right]\right)^{-1} \tag{15}$$

This is essentially the result for a tethered polymer in a homogeneous flow, with a velocity of $\tilde{\dot{\gamma}}\tilde{d}$, due to the original assumption of constant $\tilde{d}$. To obtain the correct result for shear flow, we must relax this assumption self-consistently. We still assume a linear force profile given by the combination eq 10 and eq 11, but now replace the average value of $\tilde{d}$ with the actual height at that location, $\langle \tilde{z} \rangle(n)$. The introduction of this into eq 14 yields a new eq 15, and this process can be iterated until convergence is attained.

Influence of Semiflexibility. The previous section assumed that the energy associated with the perturbation of a single link from a fully stretched orientation is completely due to the fluid flow. Semiflexible polymers, however, may also have a bending energy associated with a change in orientation. The method given above for determining the partition function of an ideal chain can also be adopted for the case of a semiflexible chain. We introduce a variable $\tilde{\kappa}_B$ that describes the bending energy of a given bond with relation to the previous bond:

$$\tilde{U}_{B,n} = \frac{\tilde{\kappa}_B}{2}(\theta_{n+1}-\theta_n)^2 \tag{16}$$

A summation of bending energy over the entire chain yields the result:

$$\sum_n^{N-1}\tilde{U}_{B,n} = \sum_n^{N-1}\frac{\tilde{\kappa}_B}{2}(\theta_{n+1}-\theta_n)^2 = \sum_n^{N-1}(\tilde{\kappa}_B\theta_n{}^2 - \tilde{\kappa}_B\theta_{n+1}\theta_n) \tag{17}$$

While this is a straightforward rewriting of the summation, it demonstrates one important characteristic of tethered semiflexible polymer chains; namely, the bending energy produces a correlation effect on adjacent beads (shown by the second term in the far right manifestation of the summation). This problem has become very difficult to solve due to the existence of these two-link interactions. To allow for an analytical solution, we use a mean field approximation and replace the value θ_{n+1} with $\langle \theta_n{}^2 \rangle_0{}^{1/2}$, which is the root-mean-square angle for a flexible chain. We can then write the entire energy of any given link:

$$\begin{aligned}\tilde{U}_n &= (\tilde{F}_{T,n} + \tilde{\kappa}_B)\theta_n{}^2 - \tilde{\kappa}\langle \theta_n{}^2 \rangle_0{}^{1/2}\theta_n \\ &= (\tilde{F}_{T,n} + \tilde{\kappa}_B)\theta_n{}^2 - \left(\frac{\tilde{\kappa}_B}{\tilde{F}_{T,n}{}^{1/2}}\right)\theta_n \\ &= A\theta_n{}^2 - B\theta_n\end{aligned} \tag{18}$$

where in the last step we define the values $A = \tilde{F}_{T,n} + \tilde{\kappa}_B$ and $B = \tilde{\kappa}_B/\tilde{F}_{T,n}{}^{1/2}$. We define a ratio that compares the mean square angle $\langle \theta_n{}^2 \rangle_0$ of a chain where $B = 0$, and the mean square angle $\langle \theta_n{}^2 \rangle$ where $B \neq 0$. This constitutes a correlation factor that describes the additional directional correlation imparted by the bending energy:

$$\begin{aligned}\frac{\langle \theta_n{}^2 \rangle}{\langle \theta_n{}^2 \rangle_0} &= \frac{\int_0^\infty \theta_n{}^3 \mathrm{e}^{-A\theta_n{}^2 + B\theta_n}\,\mathrm{d}\theta_n}{\int_0^\infty \theta_n{}^3 \mathrm{e}^{-A\theta_n{}^2}\,\mathrm{d}\theta_n} \\ &= 1 + \frac{\sqrt{\pi}y\mathrm{e}^{y^2}(1-\mathrm{erf}(y))}{2(1+\sqrt{\pi}y\mathrm{e}^{y^2}(1-\mathrm{erf}(y)))} + y^2\end{aligned} \tag{19}$$

where $y = B/(2(A)^{1/2})$ is a dimensionless comparison of the energy associated with the bending correlation to the energy associated with the uncorrelated perturbations. For the polymers in this article, where the fluid flow is large and the chain is highly elongated, we can take the limit $y \rightarrow 0$:

$$\frac{\langle \theta_n{}^2 \rangle}{\langle \theta_n{}^2 \rangle_0} \approx 1 + \frac{\sqrt{\pi}\tilde{\kappa}_B}{4(\tilde{F}_{T,n}{}^2 + \tilde{F}_{T,n}\tilde{\kappa}_B)^{1/2}} \tag{20}$$

This can then be incorporated into the calculation of $S_n[\dot{\gamma},\{z_n\}]$:

$$S_n[\dot{\gamma},\{\tilde{z}_n\}] = \frac{1}{2}\int_0^n \langle \Delta l^2 \rangle(n',\dot{\gamma},z_{n'})\frac{\langle \theta_n{}^2 \rangle}{\langle \theta_n{}^2 \rangle_0}(n',\dot{\gamma},z_{n'})\,\mathrm{d}n' \tag{21}$$

$$= \frac{1}{2}\int_0^n \frac{4}{\tilde{\dot{\gamma}}\,\tilde{d}(N-n')}\left[1 + \frac{\sqrt{\pi}\tilde{\kappa}_B}{4((\tilde{\dot{\gamma}}\,\tilde{d}(N-n'))^2 + \tilde{\dot{\gamma}}\,\tilde{d}(N-n')\tilde{\kappa}_B)^{1/2}}\right]\mathrm{d}n' \tag{22}$$

$$= \frac{1}{\tilde{\dot{\gamma}}\,\tilde{d}}\left[2\ln\left(\frac{N}{N-n}\right) + \sqrt{\pi}\left(\sqrt{1+\frac{\tilde{\kappa}_B}{\tilde{\dot{\gamma}}\,\tilde{d}(N-n)}} - \sqrt{1+\frac{\tilde{\kappa}_B}{\tilde{\dot{\gamma}}\,\tilde{d}N}}\right)\right] \tag{23}$$

This result can be incorporated into eq 4, in the same fashion as in eq 14. Furthermore, this equation can be incorporated into the equation for the average trajectory of the chain calculated for the

dx.doi.org/10.1021/ma201808c |Macromolecules 2011, 44, 9020–9028

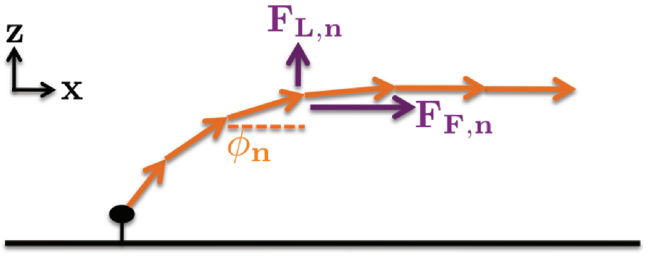

Figure 2. Introduction of hydrodynamic interactions into the geometry of a tethered polymer is accomplished by considering the lift force $F_{L,n}$ on a segment n as it compares to the net force of the flow $F_{F,n} \approx F_{T,n} - F_{T,n+1}$ on the same segment. The ratio of the two forces $F_{L,n}/F_{F,n}$ describes the direction of that given segment ϕ_n. There is a resulting z-displacement $2a\phi_n$ that can be added to the contour of the nonhydrodynamic interacting chain to yield the chain trajectory. This results in a characteristic "tether kink" like the one shown in this figure.

FJC in eq 15:

$$\langle \tilde{z} \rangle(n) = \tilde{z}_0 \left(\mathrm{erf} \left[\frac{\tilde{z}_0}{\sqrt{2S_n[\tilde{\dot{\gamma}}, \{\tilde{z}_n\}]}} \right] \right)^{-1} \tag{24}$$

which again allows for a self-consistent treatment.

Effect of HI. Traditionally, the effect of hydrodynamic interactions on, tethered polymers has largely been considered negligible.[21,23] This is due to the low density of polymer along the chain, such that screening is not a large effect, and the major dynamic effects (due to Rouse versus Zimm relaxation time scales) are incorporated naturally by considering the Weissenberg number, which scales all times by the chain relaxation time regardless of the theory used.[22] We can incorporate these effects into our theory, and identify a "tether kink" that constitutes a previously unidentified structural feature that is solely due to the hydrodynamic interactions between the polymer and the surface. This is due to the hydrodynamic lift force, an effect that has proven to be influential in near-surface hydrodynamics in work throughout the past decade.[5,11,13,16,37−40] We can incorporate the elements of recent near-surface hydrodynamic lift force theory into our theory of tethered chains in a straightforward manner.[11]

For polymer chains that lie along a plane that is parallel to the surface plane, it can be shown that the lift force at index n, $\tilde{F}_{L,n}$ is given by the equation:[11]

$$\tilde{F}_{L,n} = \sum_{i}^{N} \tilde{\mu}_{n,i} \tilde{F}_i \tag{25}$$

where the mobility describing the effect of force $\tilde{F}_i$ on the lift force $F_{L,n}$ is given by $\tilde{\mu}_{n,i} = -9r_x\tilde{d}^3(r_x^2 + 4\tilde{d}^2)^{-5/2}$ where r_x is the x-distance between bead i and a bead at position n along the chain contour.[11] Figure 2 demonstrates the main force balance that takes place on a given bead, with the tension force gradient $(\partial \tilde{F}_{T,n}/\partial n) \approx \tilde{\dot{\gamma}}\, \tilde{d} f = \tilde{F}_{F,n}$ providing a net force in the x-direction and the lift force $\tilde{F}_{L,n} = \sum_i^N \tilde{\mu}_{n,i} \tilde{\dot{\gamma}}\, \tilde{d} f$ providing a net force in the z-direction. We introduce a variable f that accounts for the lower effective shear force due to screening. This is a quasi-empirical parameter, but it will be sufficient for our purposes since most beads are in similar environments. Simulation verification of the validity of this assumption is given in the next section. We can then calculate the angle ϕ_n that a given bond will be at by the equation:

$$\phi_n = \arctan\frac{\tilde{F}_{L,n}}{\tilde{F}_{F,n}} \approx \frac{\tilde{F}_{L,n}}{\tilde{F}_{F,n}} = \frac{9\tilde{d}^3}{16} \sum_{i=1}^{N} \frac{(n-i)}{((n-i)^2 + \tilde{d}^2)^{5/2}} \tag{26}$$

A notable feature of this result is that, as long as the assumptions are met (highly stretched chain limit), the trajectory of the tethered chain at the tether point is independent of the shear rate since both the lift force and chain tension gradient are proportional to $\tilde{\dot{\gamma}}$. We can incorporate this feature into the previous formula given for the average z-coordinate of an index n:

$$\langle z \rangle(n) = \sum_{n'=1}^{n} 2a\phi_{n'} + \tilde{z}_0 \left(\mathrm{erf} \left[\frac{\tilde{z}_0}{\sqrt{2S_n[\tilde{\dot{\gamma}}, \{\tilde{z}_n\}]}} \right] \right)^{-1} \tag{27}$$

In the case of a continuous representation of the chain, the summations would simply be replaced by integrals.

DISCUSSIONS

Brownian dynamics simulations were performed to verify the validity of the analytical theory presented in the previous section. Each simulation ran for $>10^8\tau$, to ensure that good averaging was achieved. The polymer was tethered at a point $z_0 = 2a$ above the surface, and the potential diverges such that a given bead never falls below a distance a from the surface. To accomplish this, the potential used is a soft one so there is a range of values $0 < z_0 < 1$ that may be obtained depending on the overall distribution. For most of the result data, $N = 50$ and $0.1 < \tilde{\dot{\gamma}} < 10$. This ensures that the chain is in its strongly stretched limit.

For the initial state of our theory, we choose an approximate force profile:

$$F_{T,n} = \int_N^n \tilde{\dot{\gamma}} \tilde{z}_{n'}\, \mathrm{d}n' \approx \tilde{\dot{\gamma}} \tilde{d}(N-n) \tag{28}$$

that represents the tensile force along the chain for a completely straight chain. This assumption can be relaxed by self-consistently solving for $\tilde{z}_n$ by using eq 15 and eq 13. This is a well-behaved solution method, since we can show via simulation data that the approximation shown in eq 28 is very close to reality. We demonstrate this in Figure 3, where the force versus index plot is shown for a wide variety of $\tilde{\dot{\gamma}}$ for both the FD and HI cases. Ft lines representing eq 28 are shown to match well for both cases using the values $\tilde{d} = 2$ for part a, and $\tilde{d} = 3$ and $f = 0.7$ for part b (see figure). We note that this result becomes increasingly accurate as the shear rate $\tilde{\dot{\gamma}}$ gets large, due to the approach of the system to its completely stretched ground state. The choice of this ground-state geometry to describe the initial values for the set $\{\tilde{z}_n\}$ of all the z-components of the chain contour is therefore a natural one.

This initial condition is used to determine the values for $S_n[\tilde{\dot{\gamma}},\{\tilde{z}_n\}]$, $\langle \tilde{z} \rangle(n)$, and $P(n,\tilde{z})$ using eq 13, eq 14, and eq 15. A comparison of these equations and the theoretical values for these metrics can be made to simulation data. For a freely draining polymer that is a freely jointed chain, we demonstrate these comparisons in Figure 4 and Figure 5. Figure 4 demonstrates a complete fit between the theory and the z-direction probability distribution function for a wide range of values of n and $\tilde{\dot{\gamma}} = 10$

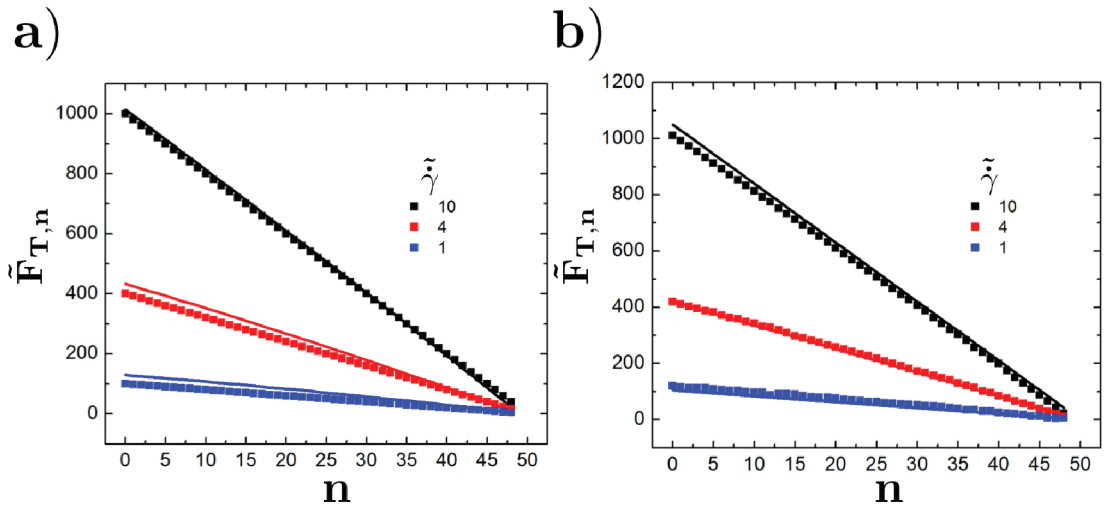

Figure 3. Tensile force $\tilde{F}_{T,n}$ as a function of the link index n for a number of shear rates $\dot{\tilde{\gamma}}$. Simulation data is given by the points, and theoretical predictions are given by the lines. Results for freely draining (a) and hydrodynamic interacting (b) are shown, with $\tilde{d} = 2$ used for FD and $\tilde{d} = 3, f = 0.7$ used for HI. Values for $\tilde{d}$ are chosen based on simulation observations.

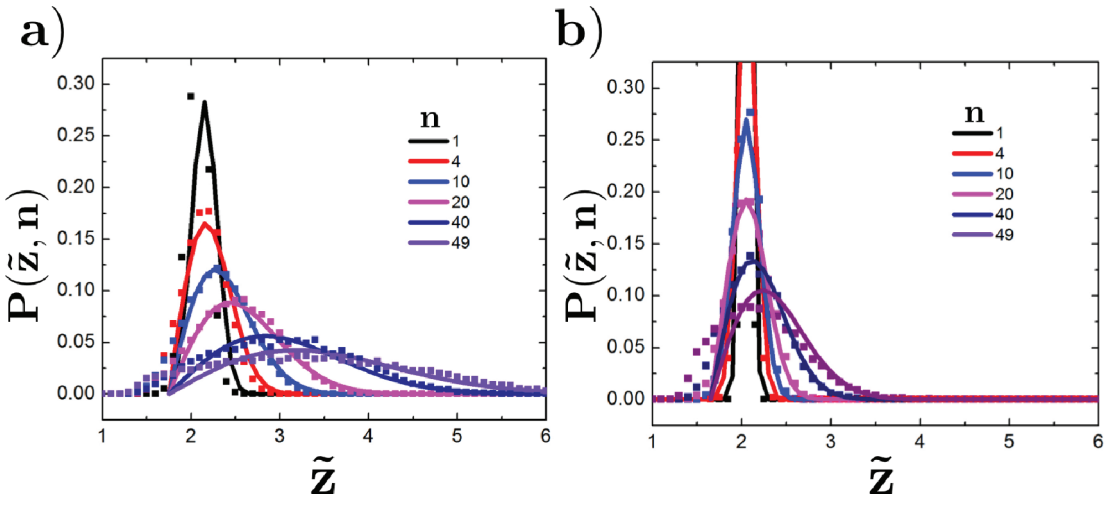

Figure 4. Normalized probability distribution functions $P(\tilde{z},n)$ as a function of the z-position of bead n for tethered chains in shear flows of $\dot{\tilde{\gamma}} = 1.0$ (a) and $\dot{\tilde{\gamma}} = 10.0$ (b). Theoretical predictions are shown by lines, and symbols represent simulation data. Because of the soft wall potential and excluded volume interactions, the surface is effectively located at $z \approx 1.5$, so z_0 is chosen to be $z_0 = 0.5$. Excellent agreement between simulation and theory is observed, with no adjustable parameters.

(Figure 4a) and 1 (Figure 4b). For both cases, it is clear that a quantitative prediction can be made using this theory, with the only significant differences between simulation and theory occurring at values of high n and low z. At these points, there is a larger than expected presence of the bead near the wall. We attribute this to two reasons: the soft potential used in modeling the wall in the simulation, which we expect would disappear by considering a much steeper wall potential, and the assumption of a linear force profile along the chain, which is less accurate at high values of n. This deviation is rather minor, however. In Figure 5a, we see that there is quantitative matching between the average chain trajectory given by both theory and simulation, without any adjustable parameters. Deviations are only seen at high n, due to the same effects described for deviations in Figure 4. This excellent agreement remains even at relatively low shear rates, demonstrating that this method offers robust prediction of tethered polymer geometries. We plot in Figure 5b the theoretical values of $S_n[\dot{\tilde{\gamma}},\{z_n\}]$ as a function of n for a number of shear rates $\dot{\tilde{\gamma}}$. This represents the time-averaged underlying geometry of the tethered chain, where a time-averaged cloud representation of a chain displays a cone-like shape at low values of n (near the tether point) that transitions to a bell-like flare at $n \sim N$. This is indeed seen in simulation, as shown by a direct qualitative comparison of theory to a cloud representation of simulation data in Figure 6. This general shape is furthermore seen universally in both experimental and simulation data from other sources, which qualitatively supports our theory (comparison of our theory to the images by Lueth and Shaqfeh is particularly striking).[21,23]

While a majority of these results are given for chains of $N = 50$, we can show that these results demonstrate the appropriate behavior even at other values of N. In Figure 7, we plot $N = 50$, 30,

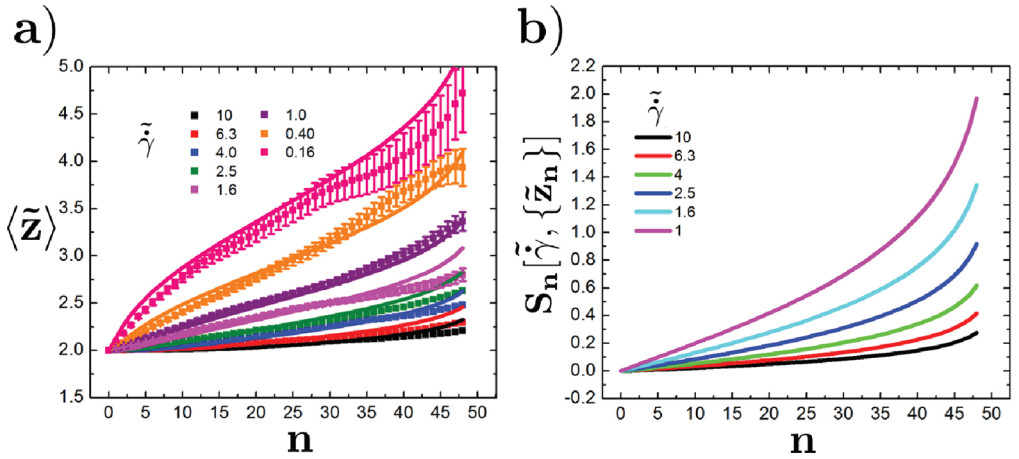

Figure 5. Mean trajectory of this polymer is shown in (a) as the $\langle\tilde{z}\rangle$ versus n, for both theory (lines) and simulation (symbols) for a wide range of $\tilde{\dot{\gamma}}$. With no adjustable parameters, it is clear that this theory is applicable over a wide range of shear rates, with the only apparent deviations occurring at large values of n. We attribute this to the soft wall potential, which results in a larger than expected tail in $P(\tilde{z},n)$ at low-z at large values of n. Error bars are shown when the error is larger than the symbol size. (b) The mean square distance from the tether point, $S_n[\tilde{\dot{\gamma}},\{\tilde{z}_n\}]$ plotted as a function of the bead index n for a number of values $\tilde{\dot{\gamma}}$. This gives an indication of the overall shape of the equilibrium, averaged polymer structure.

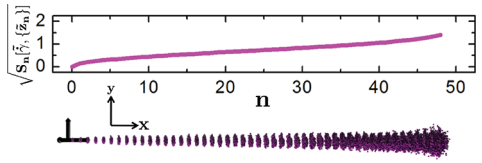

Figure 6. Plot of $(S_n[\tilde{\dot{\gamma}},\{\tilde{z}_n\}])^{1/2}$ as a function of n for a tethered polymer $N = 50$ and $\tilde{\dot{\gamma}} = 1.0$. The simulation of the same polymer under the same conditions, represented as a cloud of a large sample of visited points, is positioned below this graph and is viewed from the top-down (along the z axis). Theory predicts that the "cone" geometry of the cloud and the plotted line should follow the same curve shape. Qualitative matching can be observed upon direct visual comparison.

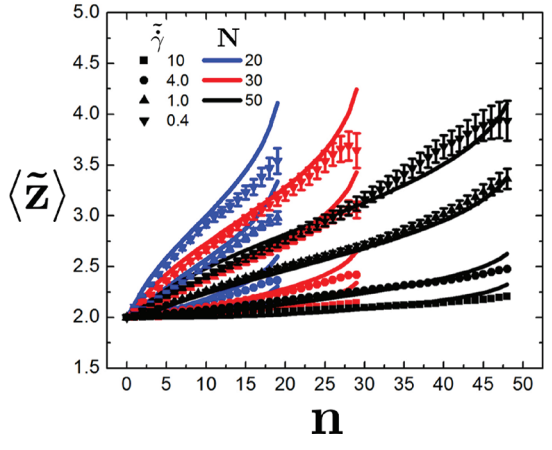

Figure 7. Average trajectory for a surface-tethered chain ($\langle\tilde{z}\rangle$ vs n) in a wide range of shear flows $\tilde{\dot{\gamma}}$ for a number of chain lengths $N = 20$, 30, and 50. Quantitative agreement between theory (lines) and simulation (symbols) is seen for all values of N, verifying the general validity of this theory. Error bars are shown when the error is larger than the symbol size.

and 20 for a number of values $\tilde{\dot{\gamma}}$. The same theory is incorporated into these results, and likewise quantitative matching is achieved with no adjustable parameters. We see that the fit is not as good at

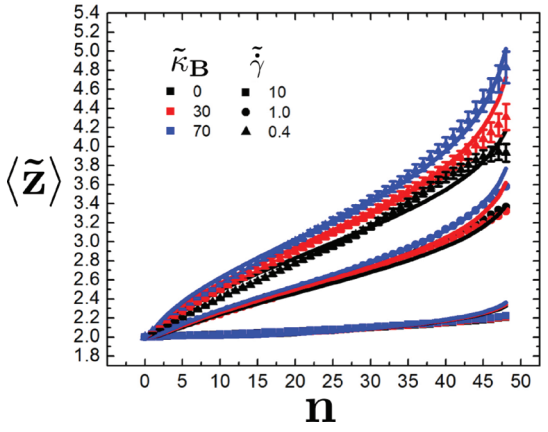

Figure 8. Average trajectory for a surface-tethered chain ($\langle\tilde{z}\rangle$ vs n) in a wide range of shear flows $\tilde{\dot{\gamma}}$ for a number of chain bending constants $\tilde{\kappa}_B$. There is quantitative agreement between theory (lines) and simulation (symbols) for all values of $\tilde{\dot{\gamma}}$ and $\tilde{\kappa}_B$, with the graph displaying the intuitive feature of having the largest geometric differences at high n and low $\tilde{\dot{\gamma}}$. Error bars are shown when the error is larger than the symbol size.

lower N, which is expected since the linear force profile assumption becomes less accurate in this limit.

The incorporation of semiflexibility into the theory also matches quantitatively to simulation results. Figure 8 demonstrates the average trajectory $\langle\tilde{z}\rangle(n)$ vs n of tethered polymers for a number of shear rates $\tilde{\dot{\gamma}}$ and bending energies $\tilde{\kappa}_B$. Unsurprisingly, the effect of rigidity on the polymer increases with decreasing shear rate. This is due to the correlation of bonds along the chain at high bending energies; the increased values of $\langle\theta_n\rangle$ bias the partition function function through the introduction of the term that is linear in θ_n in eq 18, $B = \tilde{\kappa}_B/\tilde{F}_{T,n}^{1/2}$. The form of this term is noteworthy in that it compares the bending constant $\tilde{\kappa}_B$ to the constant associated with the flow-induced straightening $\tilde{F}_{T,n}$ which is a function of n. At low n, the latter term is large and thus the difference between the FJC and the semiflexible chain is negligible. There is only a difference, therefore, once the condition is met that $\tilde{\kappa}_B \sim \tilde{F}_{T,n}^{1/2}$, which occurs at large n. This agrees qualitatively with

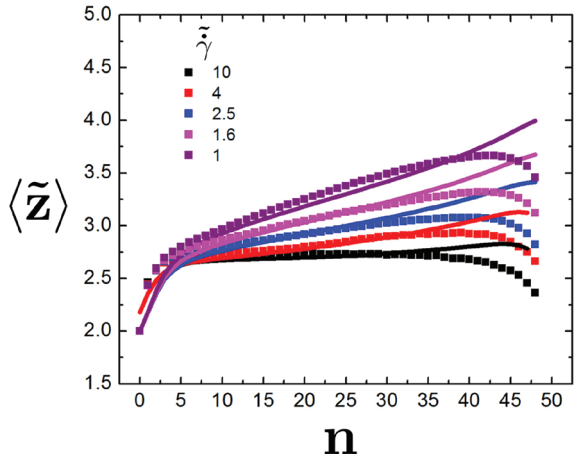

Figure 9. Average trajectory for a surface-tethered chain ($\langle \tilde{z} \rangle$ vs n) for a number of shear flows $\tilde{\dot{\gamma}}$ upon the introduction of hydrodynamic interactions. Theoretical results (lines) and simulation results (symbols) match quantitatively, in similar fashion to previous results for FD-chains. The major difference in this plot is the presence of a universal "tether kink" at low n values, which is a result of the hydrodynamic lift force. The opposite of this behavior, due to the antisymmetric nature of the hydrodynamic lift force, is seen to a lesser extent at large n where the chain end is pushed downward. Hydrodynamic screening is also present, and a value $f = 0.7$ is used to calculate the theoretical lines as determined from the results in Figure 3. Error is smaller than the symbol size.

the form of the traces in Figure 8, where there is a difference between chains with different $\tilde{\kappa}_B$ values only at the far ends of the chain.

The incorporation of hydrodynamic interactions into the simulations is also demonstrated, and we can verify that there are indeed features that are characteristic of chains with HI that are not present in FD chains. This is shown in Figure 9, which plots the trajectory $\langle \tilde{z} \rangle(n)$ versus n. While it is clear that the same general trends are followed in the overall chain trajectory compared to the FD case, HI effects importantly modify the chain behavior in the low-n trajectory. For the curves that are shown, it is apparent that this trajectory is universal and not effected by changes in $\tilde{\dot{\gamma}}$. This is predicted by the theory, which again demonstrates quantitative matching with the simulation data. We stress that this universal trajectory is entirely due to the geometrical parameters, and the lift force only plays a major role at the ends of the polymer due to the semi-infinite geometry. Away from the ends, a given monomer feels the effects of surrounding monomers that appear to extend quasi-infinitely in both directions, and therefore feels no lift force due to the antisymmetry of the HI tensor around a point force. It is also important to note that a discretized calculation is done in this case; in the case of a real polymer, we expect that a continuous representation would be more appropriate. Finally, we can incorporate in an effective manner the effect of screening on the polymer chain. This is apparent by considering Figure 3, which shows that the force profile along the chain is approximately linear, much like the case of a FD polymer. The presence of HI, however, results in considerable screening effects such that a "screening factor" f describes the potency of the shear flow. From fitting the simulation data in Figure 3, we obtain the result $f \approx 0.7$, which is what is successfully used in the above theory.

CONCLUSIONS

We have developed a model describing, without adjustable parameters, the geometry of a polymer that is tethered to a surface in the presence of a shear flow. This model accurately reproduces simulation results for both the average trajectory of the chain in space and also the time-averaged spatial distribution of monomers around this average trajectory. When hydrodynamic effects are included, a previously unobserved "tether kink" feature is predicted.

The theory described in this paper is based on the idea that a tethered polymer that is held in shear flow can be well-represented by creating an analogy with point-source diffusion near a surface. As long as the partition function of a given link can be represented as a function of n, an analytical expression for the distribution function of the z-coordinate can be developed in a self-consistent manner. This theory provides quantitative predictions for chain geometry as a function of shear rate $\tilde{\dot{\gamma}}$ by considering the partition function for the deviation of individual bonds from the fully stretched ground-state in a freely jointed chain, and then treating these deviations as steps in a random-walk diffusion process from the tether point. A simple mean-field type model is used to account for short-range correlations between adjacent links in the case of a semiflexible chain. The model used for semiflexibility in these simulations can be translated into the parameters of a worm-like chain in a straightforward manner.[41] The deviations of this chain from the FJC is captured by the dimensionless value of the parameter B, which compares the energy associated with bending energy to the energy associated with fluid flow drag forces. Finally, the effect of hydrodynamic interactions is incorporated into the model by considering the implications of screening and lift forces on the equilibrium structure of the tethered chain. We develop theory and simulation to describe the universal "tether kink" geometry and demonstrate that it is independent of shear for high shear rates.

Tethered chains in the presence of a shear flow is an important problem that has implications in surface functionalization, microfluidic control of single-chain polymers, and perhaps most importantly, adsorption phenomena. This article introduces important effects for the latter, especially. It has long been known that the adsorption and desorption of chains in the presence of fluid flows involves a competition between hydrodynamic lift and favorable surface interactions.[16,31] Since a partially adsorbed chain resembles the geometry of a tethered chain, our results elucidate the forces present on such a chain due to the hydrodynamics. In particular, a full accounting of the lift force in the context of this geometry shows that its effect on a chain will only be upward and non-negligible in the vicinity of the tether point. This means that there is no lift force to prevent readsorption of the desorped chain segment away from the tether point, and in fact our results reveal that the "lift force" is actually toward the surface at the free chain end such that readsorption may be enhanced.

AUTHOR INFORMATION

Corresponding Author

*E-mail: aalexand@mit.edu.

ACKNOWLEDGMENT

We would like to acknowledge financial support from the National Defense Science and Engineering Graduate Fellowship and from an NSF CAREER Award No. 1054671. We also

gratefully acknowledge stimulating discussions and feedback from Prof. G. C. Rutledge.

REFERENCES

(1) Kim, Y. W.; Netz, R. R. *Phys. Rev. Lett.* **2006**, *96*, 158101.
(2) Irvine, D. J.; Mayes, A. M.; Satija, S. K.; Barker, J. G.; Sofia-Allgor, S. J.; Griffith, L. G. *J. Biomed. Mater. Res.* **1998**, *40*, 498–509.
(3) Doyle, P. S.; Ladoux, B.; Viovy, J. L. *Phys. Rev. Lett.* **2000**, *84*, 4769–4772.
(4) Jeppesen, C.; Wong, J. Y.; Kuhl, T. L.; Israelachvili, J. N.; Mullah, N.; Zalipsky, S.; Marques, C. M. *Science* **2001**, *293*, 465–468.
(5) Jendrejack, R. M.; Schwartz, D. C.; de Pablo, J. J.; Graham, M. D. *J. Chem. Phys.* **2004**, *120*, 2513–2529.
(6) Klein, J.; Kumacheva, E.; Mahalu, D.; Perahia, D.; Fetters, L. J. *Nature* **1994**, *370*, 634–636.
(7) Elbert, D.; Hubbell, J. *Annu. Rev. Mater. Sci.* **1996**, *26*, 365–394.
(8) Reeves, D.; Cheveralls, K.; Kondev, J. *Phys. Rev. E* **2011**, *84*, 021914.
(9) Balducci, A.; Doyle, P. S. *Macromolecules* **2008**, *41*, 5485–5492.
(10) Braun, E.; Eichen, Y.; Sivan, U.; Ben-Yoseph, G. *Nature* **1998**, *391*, 775–778.
(11) Sing, C. E.; Alexander-Katz, A. *Europhys. Lett.* **2011**, 48001.
(12) Buguin, A.; Brochard-Wyart, F. *Macromolecules* **1996**, *29*, 4937–4943.
(13) Sendner, C.; Netz, R. R. *EPL-Europhys. Lett.* **2008**, *81*, 54006.
(14) Serr, A.; Netz, R. R. *EPL-Europhys. Lett.* **2007**, *78*, 68006.
(15) DeGennes, P. G. *Macromolecules* **1980**, *13*, 1069–1075.
(16) Hoda, N.; Kumar, S. *J. Chem. Phys.* **2008**, *128*, 164907.
(17) Szymczak, P.; Cieplak, M. *J. Chem. Phys.* **2007**, *127*, 155106.
(18) Brochard-Wyart, F. *Europhys. Lett.* **1993**, *23*, 105–111.
(19) Perkins, T. T.; Smith, D. E.; Larson, R. G.; Chu, S. *Science* **1995**, *268*, 83–87.
(20) Schroeder, C. M.; Teixeira, R. E.; Shaqfeh, E. S. G.; Chu, S. *Phys. Rev. Lett.* **2005**, *95*, 018301.
(21) Ladoux, B.; Doyle, P. S. *Europhys. Lett.* **2000**, *52*, 511–517.
(22) Ibanez-Garcia, G. O.; Hanna, S. *Soft Matter* **2009**, *5*, 4464–4476.
(23) Lueth, C. A.; Shaqfeh, E. S. G. *Macromolecules* **2009**, *42*, 9170–9182.
(24) Zhang, Y.; Donev, A.; Weisgraber, T.; Alder, B. J.; Graham, M. D.; de Pablo, J. J. *J. Chem. Phys.* **2009**, *130*, 234902.
(25) Gratton, Y.; Slater, G. W. *Eur. Phys. J. E* **2005**, *17*, 455–465.
(26) Delgado-Buscalioni, R. *Phys. Rev. Lett.* **2006**, *96*, 088303.
(27) Chertkov, M.; Kolokolov, I.; Lebedev, V.; Turitsyn, K. *J. Fluid Mech.* **2005**, *531*, 251–260.
(28) Winkler, R. G. *Phys. Rev. Lett.* **2006**, *97*, 128301.
(29) Gerashchenko, S.; Steinberg, V. *Phys. Rev. Lett.* **2006**, *96*, 038304.
(30) He, G.-L.; Messina, R.; Loewen, H.; Kiriy, A.; Bocharova, V.; Stamm, M. *Soft Matter* **2009**, *5*, 3014–3017.
(31) Serr, A.; Sendner, C.; Mueller, F.; Einert, T. R.; Netz, R. R. *EPL-Europhys. Lett.* **2010**, *92*, 38002.
(32) Blake, J. R.; Chwang, A. T. *J. Eng. Math.* **1974**, *8*, 23–29.
(33) Blake, J. R. *Proc. Cambridge Philos. Soc.* **1971**, *70*, 303–310.
(34) Rotne, J.; Prager, S. *J. Chem. Phys.* **1969**, *50*, 4831.
(35) Yamakawa, H. *J. Chem. Phys.* **2003**, *53*, 436–443.
(36) Sing, C. E.; Schmid, L.; Schneider, M. F.; Franke, T.; Alexander-Katz, A. *Proc. Natl. Acad. Sci. U.S.A.* **2010**, *107*, 535–540.
(37) Sendner, C.; Netz, R. R. *EPL-Europhys. Lett.* **2007**, *79*, 58004.
(38) Fang, L.; Hu, H.; Larson, R. G. *J. Rheol.* **2005**, *49*, 127–138.
(39) Jendrejack, R. M.; Dimalanta, E. T.; Schwartz, D. C.; Graham, M. D.; de Pablo, J. J. *Phys. Rev. Lett.* **2003**, *91*, 038102.
(40) Park, J.; Bricker, J. M.; Butler, J. E. *Phys. Rev. E* **2007**, *76*, 040801.
(41) Rubinstein, M.; Colby, R. H. *Polymer Physics*; Oxford Univ. Press: Oxford, U.K., 2003.